SUPPLEMENTARY INFORMATION

Photocyclic behavior of rhodopsin induced by a novel isomerization mechanism

Sahil Gulati[a,b], Beata Jastrzebska[a,b], Surajit Banerjee[c], Ángel L. Placeres[d], Przemyslaw Miszta[e], Songqi Gao[a], Karl Gunderson[f], Gregory Tochtrop[d], Slawomir Filipek[e], Kota Katayama[a*], Philip D. Kiser[a, g], Muneto Mogi[f], Phoebe L. Stewart[a,b], Krzysztof Palczewski[a,b*]

[a]Department of Pharmacology, School of Medicine, Case Western Reserve University, 10900 Euclid Avenue, Cleveland, OH 44106, USA

[b]Cleveland Center for Membrane and Structural Biology, Case Western Reserve University, 1819E 101st Street, Cleveland, OH 44106, USA

[c]Department of Chemistry and Chemical Biology, Cornell University, Ithaca, NY 14850, and Northeastern Collaborative Access Team, Argonne National Laboratory, Argonne, IL 60439

[d]Department of Chemistry, Case Western Reserve University, 10900 Euclid Avenue, Cleveland, Ohio 44106, USA

[e]Faculty of Chemistry, Biological and Chemical Research Centre, University of Warsaw, Krakowskie Przedmiescie 26/28, 00-927 Warszawa, Poland

[f]Novartis Institutes for BioMedical Research Inc., 100 Technology Square, Cambridge, MA 02139, USA

[g]Research Service, Louis Stokes Cleveland VA Medical Center, Cleveland, OH 44106, USA

[*]Corresponding authors: Department of Pharmacology, School of Medicine, Case Western Reserve University, 10900 Euclid Avenue, Cleveland, OH 44106, USA, kxp65@case.edu; kxk477@case.edu

Table of Contents:

1. Extended results……..S3

2. NMR characterization of 6mr isomers……..S5

3. Supplementary tables……. S7

4. Supplementary figure legends……...S12

5. References…….....S15

Extended results:

Molecular mechanics (MM) calculations: MM analyses were performed to obtain a plot revealing changes in the energy of inactive Rh structure docked with the 11-*cis* 6mr isomer upon rotation of its C^{12}-C^{13}-C^{14}-C^{15} dihedral angle (Figs. *2C*, *S8*). The 6-membered ring of 6mr tended to preferentially rotate anticlockwise (from K296 towards 6mr) during our calculations. The obtained energy minima during this anticlockwise rotation of C^{12}-C^{13}-C^{14}-C^{15} dihedral angle were 170°, -11°, and -193° with energies of -811, -798, and -815 kcal/mol, respectively (Figs. *2C*, *S8*, *label 0, II, and IV, respectively*). For the clockwise rotation, the minima were 351° (-9°) and 532° (172°) with energies of -787 and -810 kcal/mol, respectively (Fig. *S8*, *label -II and -IV, resp.*). The maxima for the anticlockwise rotation were 73° (-711 kcal/mol) and -132° (-701 kcal/mol) (Figs. *2C*, *S8*, *label I and III, respectively*), and for the clockwise rotation were 270° (-90°) and 496° (136°) with corresponding energies of -695 and -715 kcal/mol (Fig. *S8*, *label -I and -III, respectively*).

The 6mr C^{12}-C^{13}-C^{14}-C^{15} dihedral energy plot indicates that the initial dihedral angle is 170°, 10° lower than the starting angle for the rotation scan which is 180° for the C^{12}-C^{13}-C^{14}-C^{15} dihedral angle (Figs. *2C*, *S8*, *label 0*). This facilitates isomerization of the 11-*cis* 6mr isomer into the 11,13-*dicis* form along the C^{13}=C^{14} double bond. The energy plot also features a 16 kcal/mol lower energy maximum during the anticlockwise rotation as compared to the clockwise rotation (see Fig. *S8*, *label I and -I*). These results indicate that the anticlockwise rotation of the C^{12}-C^{13}-C^{14}-C^{15} dihedral angle is preferred over the clockwise rotation.

The first energy maximum during the anticlockwise rotation (73°, *label I*) is associated with breaking of the interaction between the protonated Schiff base (PSB) and E113 during gradual isomerization of C^{13}=C^{14}, releasing the strain on the 6mr (the PSB is rotated about 90°). The rotation of the C^{13}=C^{14} bond is accompanied by a much smaller rotation of the 6-membered ring (about 40° as compared to its initial position) which returns back to its initial position at about 0°. At the same angle, the PSB is rotated by an additional 90° and remains pointing away from E113. This conformation approaches the energy minimum at -11° (see *label II*). During subsequent rotation of the C^{20}-C^{13}-C^{14}-C^{15} dihedral angle, the PSB gradually rotates and forms a hydrogen bond linking E181 via Wat 2a to reach the first energy maximum at -124° (see *label III', open circle*). The second energy maximum at -132° (see *label III*) is associated with breaking of this interaction and immediate formation of a direct salt bridge between the PSB and E113.

Overall, the 11,13-*dicis* to 11-*cis* re-isomerization involving a 360° rotation of the C^{12}-C^{13}-C^{14}-C^{15} dihedral angle is energetically plausible since the energy minimum after a half rotation at -11° (*label II*) is higher than the initial minimum at 170° (*label 0*).

During clockwise rotation there is a separation between a flip of the PSB and release of strain on 6mr. First, the 6mr undergoes a rotation of about 90° at 262° (small energy minimum, *label –I' open circle*) which is followed by the PSB flip from E113 to E181 with Wat 2a bridging this connection. Second, the release of strain on 6mr happens at 270° (*label -I*). In the energy minimum at 351° (*label -II*), the PSB does not form a salt bridge with either E113 or E181. A

separation between the PSB flip and the release of retinal strain is even larger for the second energy maximum which includes a 180° flip of the PSB and restoration of a salt bridge with E113 (at 415°, *label -III' open circle*). There is a continuous increase of energy during isomerization from 11,13-*dicis* to the 11-*cis* 6mr isomer that culminates at 496° (*label -III*) with the release of retinal strain.

We also calculated the energies of inactive Rh and the active Meta-II state docked with the 11-*cis* and 11,13-*dicis* 6mr isomers, separately and without any restraints. The inactive Rh model with 11-*cis* 6mr isomer (Fig. *S9A*) had an energy minimum of -852 kcal/mol (with the C^{12}-C^{13}-C^{14}-C^{15} dihedral angle being 174°). In contrast, the inactive Rh model docked instead with the 11,13-*dicis* 6mr isomer (Fig. *S9B*) manifested a higher energy minimum of -832 kcal/mol (dihedral angle -10°). Therefore, the 11-*cis* isomer of 6mr energetically fits better to the inactive state of Rh. Interestingly, the C^{12}-C^{13}-C^{14}-C^{15} dihedral angles of the 11-*cis* and 11,13-*dicis*-bound inactive Rh models (174° and -10°, respectively) are similar to those obtained from the C^{12}-C^{13}-C^{14}-C^{15} energy plot analysis (Fig. *S8*) (170° and -11°, respectively). In contrast, the active Meta-II structure docked with the 11-*cis* 6mr isomer (Fig. *S9C*) had an energy minimum at -838 kcal/mol (dihedral angle -173°), and with the 11,13-*dicis* isomer (Fig. *S9D*) at -835 kcal/mol (dihedral angle 1°). The difference in energy minima of the active Meta-II state complexed with the 11-*cis* and 11,13-*dicis* 6mr isomers is only 3 kcal/mol, significantly smaller than the difference found for inactive Rh (20 kcal/mol). This 3 kcal/mol energy gap can easily be overcome by small changes in the microenvironment of Rh mediated by water and lipid dynamics.

NMR characterization of the 6mr isomers:

9,11,13-*tricis* 6mr isomer (Peak 1: (7E,9Z,11Z,13Z)-cyclohexyl-[1',2':10,13]-retinal)

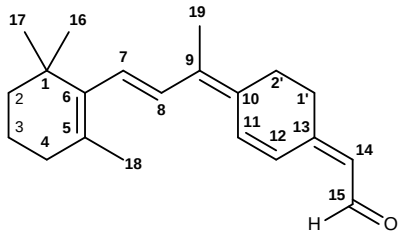

^{1}H-NMR (500 MHz, C_6D_6): δ 1.10 (s, 6H, C-16,17), 1.44-1.50 (m, 2H, C-2), 1.55-1.62 (m, 2H, C-3), 1.70 (s, 3H, C-19), 1.76 (s, 3H, C-18), 1.96 (t, 2H, *J* = 5.9 Hz, C-4) 2.03 (t, 2H, *J* = 7.0 Hz, C-1'), 2.15 (t, 2H, *J* = 6.9 Hz, C-2'), 5.65 (d, 1H, *J* = 7.7 Hz, C-14), 6.32 (d, 1H, *J* = 15.9 Hz, C-7), 6.69 (d, 1H, *J* = 10.1 Hz, C-12), 6.80 (d, 1H, *J* = 15.9 Hz, C-8), 6.86 (d, 1H, *J* = 10.0 Hz, C-11), 10.12 (d, 1H, *J* = 7.7 Hz, C-15).

11,13-*dicis* 6mr isomer (Peak 2: (7E,9E,11Z,13Z)-cyclohexyl-[1',2':10,13]-retinal)

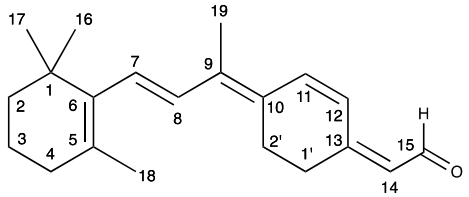

^{1}H-NMR (500 MHz, C_6D_6): δ 1.10 (s, 6H, C-16,17), 1.43-1.50 (m, 2H, C-2), 1.54-1.62 (m, 2H, C-3), 1.75 (s, 3H, C-18), 1.80 (s, 3H, C-19), 1.96 (t, 2H, *J* = 6.1 Hz, C-4), 2.00 (t, 2H, *J* = 7.0 Hz, C-1'), 2.30 (t, 2H, *J* = 6.9 Hz, C-2'), 5.62 (d, 1H, *J* = 7.6 Hz, C-14), 6.40 (d, 1H, *J* = 15.9 Hz, C-7), 6.59-6.66 (overlapping doublets, 2H, C-8 + C-11), 6.78 (d, 1H, *J* = 10.1 Hz, C-12), 10.13 (d, 1H, *J* = 7.7 Hz, C-15).

11-*cis* 6mr isomer (Peak 3: (7E,9E,11Z,13E)-cyclohexyl-[1',2':10,13]-retinal)

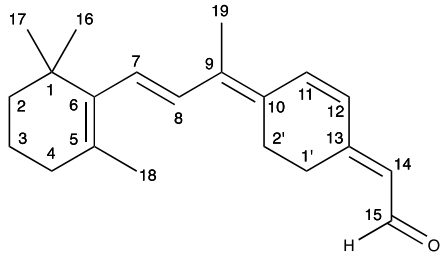

^{1}H-NMR (500 MHz, C_6D_6): δ 1.12 (s, 6H, C-16,17), 1.44-1.51 (m, 2H, C-2), 1.55-1.63 (m, 2H, C-3), 1.76 (s, 3H, C-19), 1.78 (s, 3H, C-18), 1.97 (t, 2H, *J* = 6.0 Hz, C-4), 2.22 (t, 2H, *J* = 6.8 Hz, C-2'), 2.32 (t, 2H, *J* = 6.7 Hz, C-1'), 5.83 (d, 1H, *J* = 9.8 Hz, C-12), 5.88 (d, 1H, *J* = 8.1 Hz, C-14), 6.41 (d, 1H, *J* = 15.9 Hz, C-7), 6.60 (d, 1H, *J* = 9.7 Hz, C-11), 6.66 (d, 1H, *J* = 15.9 Hz, C-8), 9.95 (d, 1H, *J* = 8.1 Hz, C-15).

9,11-*dicis* 6mr isomer (Peak 4: (7E,9Z,11Z,13E)-cyclohexyl-[1',2':10,13]-retinal)

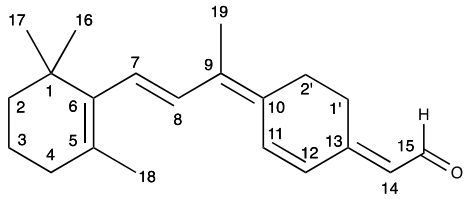

^{1}H-NMR (500 MHz, C_6D_6): δ 1.10 (s, 6H, C-16,17), 1.41-1.51 (m, 2H, C-2), 1.53-1.63 (m, 2H, C-3), 1.71 (s, 3H, C-19), 1.74 (s, 3H, C-18), 1.95 (t, 2H, *J* = 5.9 Hz, C-4), 2.08 (t, 2H, *J* = 7.1 Hz, C-2'), 2.37 (t, 2H, *J* = 6.7 Hz, C-1'), 5.77 (d, 1H, *J* = 9.8 Hz, C-12), 5.85 (d, 1H, *J* = 7.9 Hz, C-14), 6.32 (d, 1H, *J* = 15.8 Hz, C-7), 6.78 (d, 1H, *J* = 15.9 Hz, C-8), 6.85 (d, 1H, *J* = 9.8 Hz, C-11), 9.97 (d, 1H, *J* = 8.0 Hz, C-15).

Table S1. Proton table of the 9,11,13-*tricis* 6mr isomer (Peak 1: (7E,9Z,11Z,13Z)-cyclohexyl-[1',2':10,13]-retinal).

№	δ_H (mult, *J* in Hz)
1	-
2	1.44-1.50 (m)
3	1.55-1.62 (m)
4	1.96 (t, 5.9)
5	-
6	-
7	6.32 (d, 15.9)
8	6.80 (d, 15.9)
9	-
10	-
11	6.86 (d, 10.0)
12	6.69 (d, 10.1)
13	-
14	5.65 (d, 7.7)
15	10.12 (d, 7.7)
16	1.10 (s)
17	1.10 (s)
18	1.76 (s)
19	1.70 (s)
1'	2.03 (t, 7.0)
2'	2.15 (t, 6.9)

Table S2. Proton table of the 11,13-*dicis* 6mr isomer (Peak 2: (7E,9E,11Z,13Z)-cyclohexyl-[1',2':10,13]-retinal).

№	δ_H (mult, *J* in Hz)
1	-
2	1.42-1.52 (m)
3	1.54-1.64 (m)
4	1.96 (t, 5.9)
5	-
6	-
7	6.33 (d, 15.8)
8	6.79 (d, 15.9)
9	-
10	-
11	6.86 (d, 9.8)
12	5.78 (d, 9.8)
13	-
14	5.86 (d, 7.9)
15	9.98 (d, 8.0)
16	1.11 (s)
17	1.11 (s)
18	1.75 (s)
19	1.72 (s)
1'	2.38 (t, 6.7)
2'	2.09 (t, 7.1)

Table S3. Proton table of the 11-*cis* 6mr isomer (Peak 3: (7E,9E,11Z,13E)-cyclohexyl-[1',2':10,13]-retinal).

№	δ_H (mult, *J* in Hz)
1	-
2	1.44-1.51 (m)
3	1.55-1.63 (m)
4	1.97 (t, 6.0)
5	-
6	-
7	6.41 (d, 15.9)
8	6.66 (d, 15.9)
9	-
10	-
11	6.60 (d, 9.7)
12	5.83 (d, 9.8)
13	-
14	5.88 (d, 8.1)
15	9.95 (d, 8.1)
16	1.12 (s)
17	1.12 (s)
18	1.78 (s)
19	1.76 (s)
1'	2.32 (t, 6.7)
2'	2.22 (t, 6.8)

Table S4. Proton table of the 9,11-*dicis* 6mr isomer (Peak 4: (7E,9Z,11Z,13E)-cyclohexyl-[1',2':10,13]-retinal).

№	δ_H (mult, *J* in Hz)
1	-
2	1.41-1.51 (m)
3	1.53-1.63 (m)
4	1.95 (t, 5.9)
5	-
6	-
7	6.32 (d, 15.8)
8	6.78 (d, 15.9)
9	-
10	-
11	6.85 (d, 9.8)
12	5.77 (d, 9.8)
13	-
14	5.85 (d, 7.9)
15	9.97 (d, 8.0)
16	1.10 (s)
17	1.10 (s)
18	1.74 (s)
19	1.71 (s)
1'	2.37 (t, 6.7)
2'	2.08 (t, 7.1)

Table S5. Diffraction data collection and structural refinement statistics for Rh6mr and opsin.

Data collection		
	Rh6mr	**Opsin**
Beamline	NE-CAT 24-ID-C	NE-CAT 24-ID-C
Space group	$P3_121$	$H32$
Unit cell parameters (Å)	a = 81.72; c = 200.01	a = 242.66; c = 111.77
Wavelength (Å)	0.97920	0.97890
Resolution (Å)†	58.5-4.01 (4.25-4.01)	50-2.7 (2.77-2.70)
Unique reflections†	6944 (1081)	34545 (2530)
Completeness (%)†	99.8 (99.5)	100 (100)
Multiplicity†	10.6 (10.91)	22.8 (15.5)
$\langle I/\sigma I \rangle$†	6.33 (0.36)	20.9 (0.74)
$R_{meas}I$ (%)†#	24.3 (562.5)	12.4 (565.7)
$CC_{1/2}$ (%) †	99.9 (49.0)	99.9 (54.6)
Wilson *B*-factor (Å^2)	182.06	92.9
Structure refinement		
Resolution (Å)	4.01	2.7
R_{work}/R_{free} (%)	31/36	23/26
No. of atoms		
Protein	2746	2606
Ligands	24	154
Water	N.A.	32
<B-factors> (Å^2)		
Overall	308.687	95.262
Atoms of protein	309.311	93.861
Atoms of solvent water	N.A.	80.515
RMS deviations		
Bond lengths (Å)	0.0094	0.0052
Bond angles (°)	1.2291	1.0296
Ramachandran statistics		
Ramachandran		
Favored (%)	91.04	95.08
Outliers	0	0
Molprobity score	1.88	1.25

†Values in parentheses are for the highest-resolution shell of data. APS, Advanced Photon Source; ID, insertion device.

Supplementary figure legends

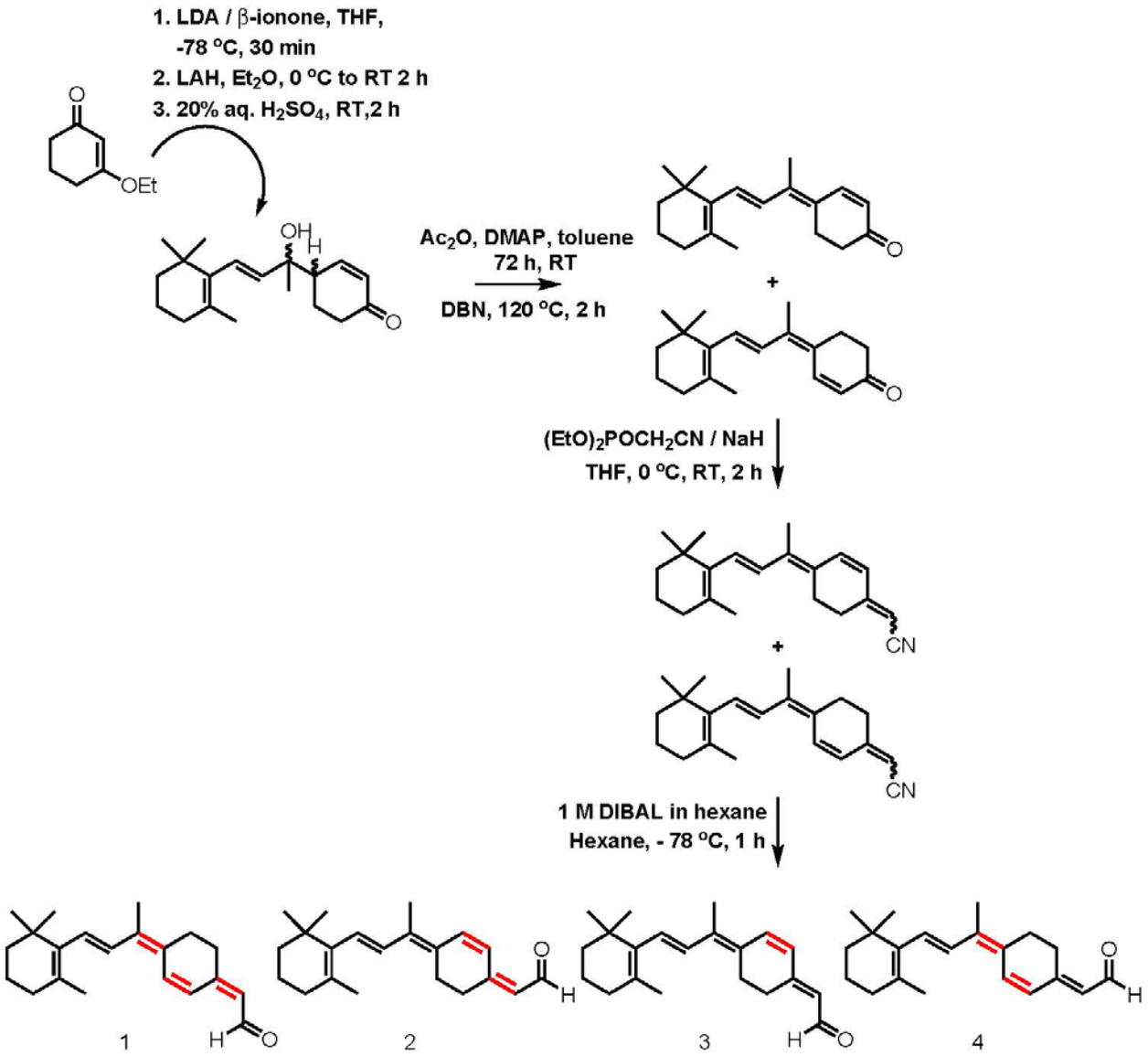

Figure S1. Synthesis of 6mr isomers. Retinoids were prepared by a method reported by Bhattacharya *et al.(1)* The identity and purity of the 6mr isomers were confirmed by both NMR and normal-phase HPLC as described in Materials and Methods.

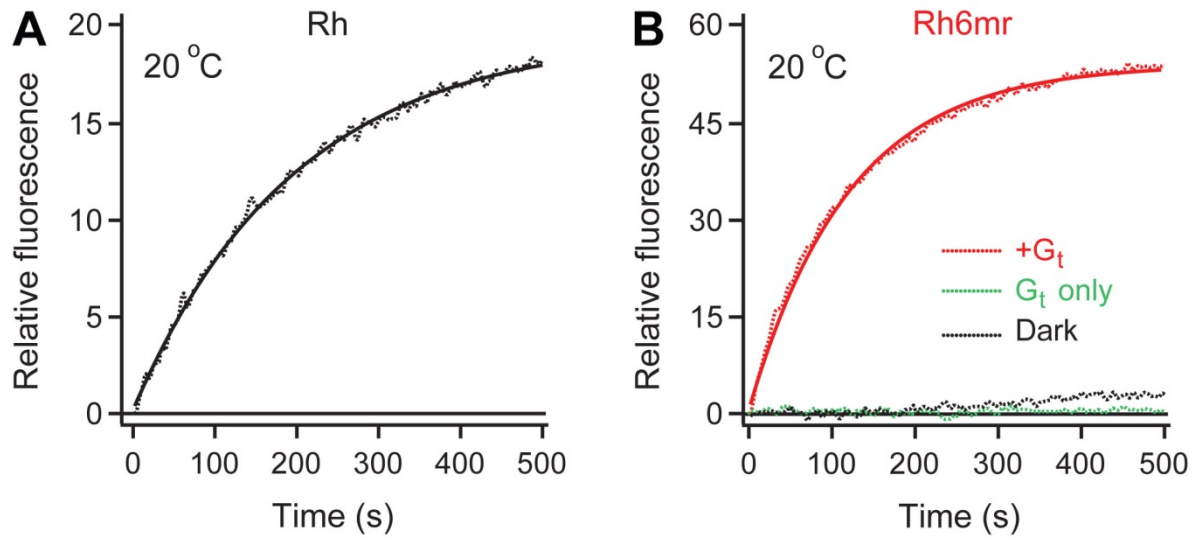

Figure S2. G_t activation by activated Rh and Rh6mr. (A) The G_t activation ability of Rh was determined by the increase in G_t alpha subunit intrinsic tryptophan fluorescence in the presence of light-activated Rh at 20 °C, pH 7.0. (B) G_t activation by light-activated Rh6mr. No exponential increase in the G_t alpha subunit fluorescence was observed in the absence of either active Rh6mr (*green*) or light stimuli (*black dashes*).

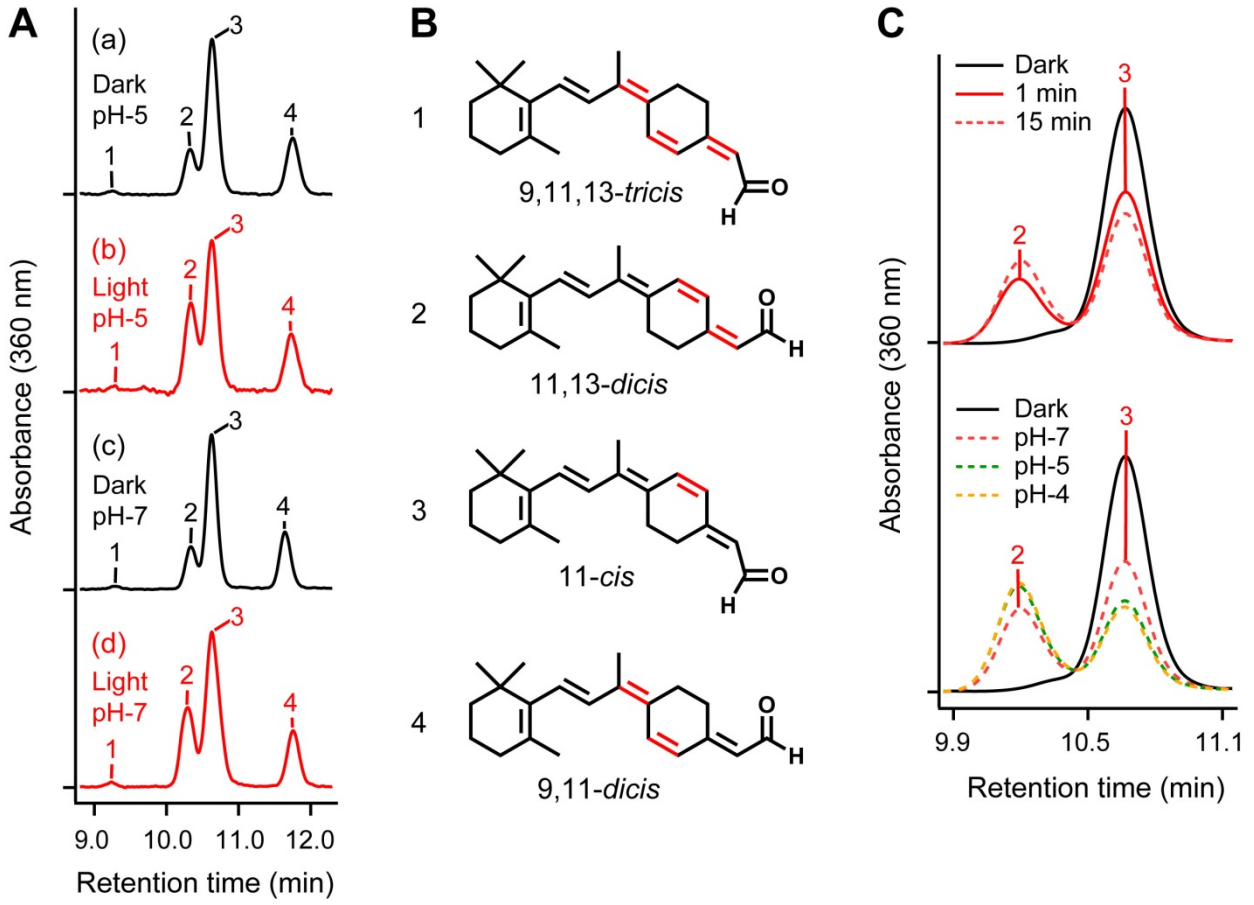

Figure S3. HPLC analysis of Rh6mr and the chemical structures of 6mr isomers. (A) Extraction of 6mr-oximes from Rh6mr under both dark (*black*) and light (*red*) conditions was carried out with hexanes after opsin denaturation in the presence of methanol and 100 mM hydroxylamine at 4 °C, either at pH 5.0 or 7.0. HPLC chromatograms of the extracted retinal-oximes from Rh6mr are shown in the dark at pH 5.0 (a) and pH 7.0 (c), and after a 1 min illumination with 480-520 nm light at either pH 5.0 (b) or pH 7.0 (d). (B) Chemical structures of the four 6mr isomers. (C) The effect of prolonged illumination and pH on the formation of 11,13-*dicis*-bound Rh6mr. HPLC chromatograms of Rh6mr regenerated with pure 11-*cis* 6mr isomer. (*Top*) HPLC analysis under the dark (*black*), after 1 min (*red solid*) and 15 min (*red dashes*) illumination at pH 7.0 revealed continuous isomerization of 11-*cis* 6mr isomer to the 11,13-*dicis* isomer. (*Bottom*) The formation of 11,13-*dicis* 6mr isomer is further potentiated in acidic conditions. HPLC chromatograms of the extracted retinal-oximes from Rh6mr are shown in the dark (*black*), and after 15 min illumination at pH 7.0 (*red dashes*), 5.0 (*green dashes*) and 4.0 (*yellow dashes*).

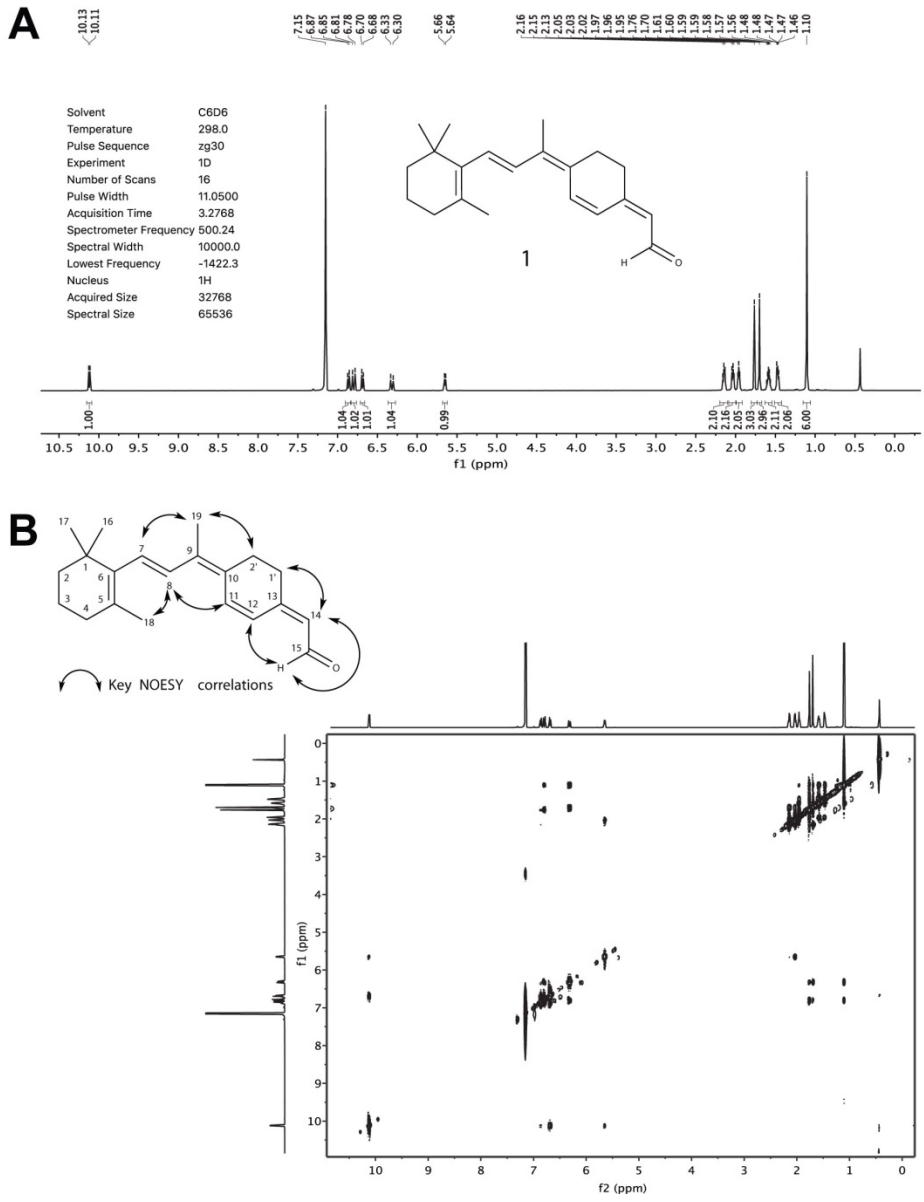

Figure S4. NMR characterization of the 9,11,13-*tricis* isomer of 6mr (peak 1). ^{1}H (A) and NOESY (B) NMR spectra were acquired at 25 °C, and referenced relative to the residual proton resonances of C6D6 (δ= 7.15 ppm). The 9,11,13-*tricis* 6mr isomer was purified by normal-phase HPLC and 1.9 mg of the purified isomer was analyzed.

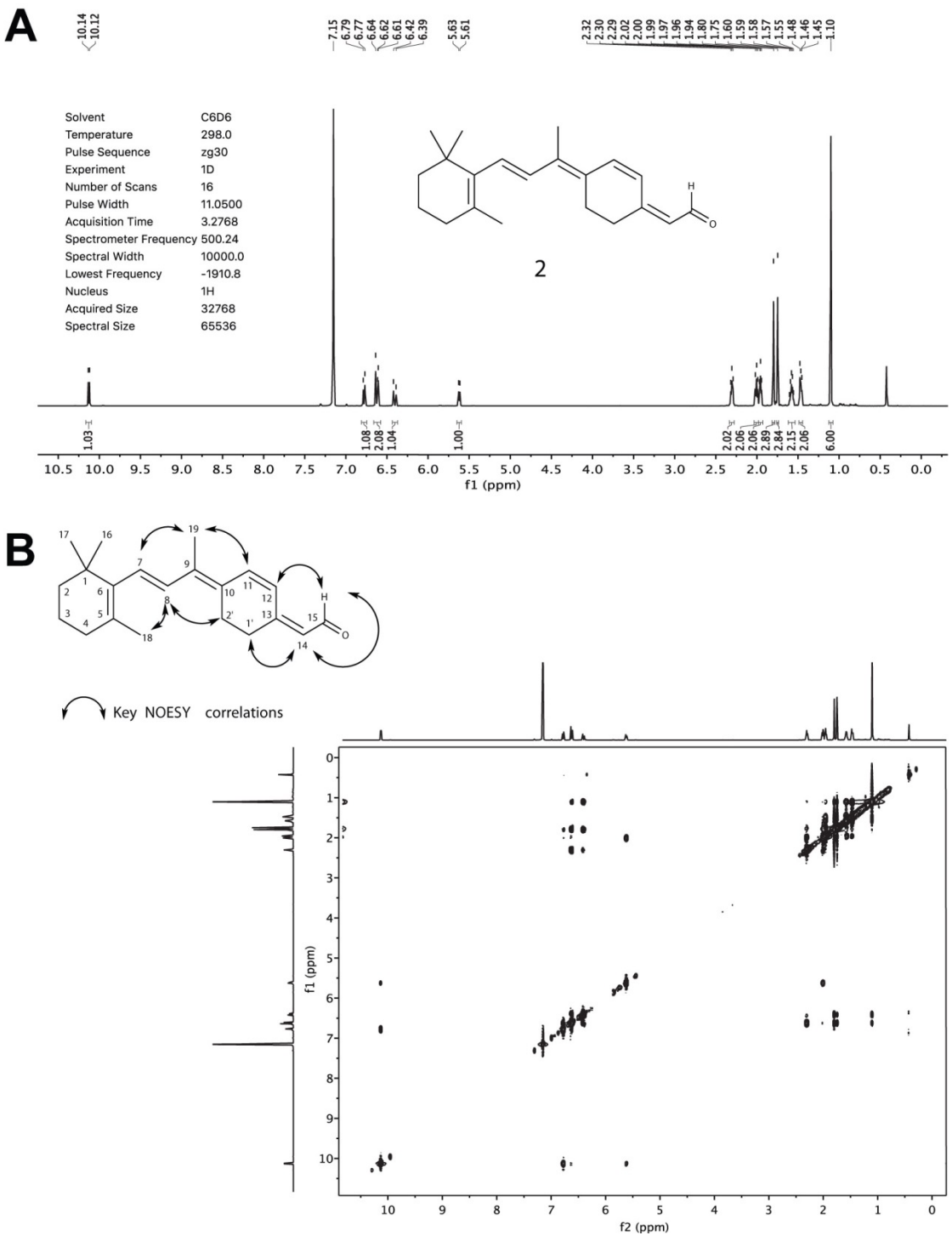

Figure S5. NMR characterization of the 11,13-*dicis* isomer of 6mr (peak 2). ^{1}H (A) and NOESY (B) NMR spectra were acquired at 25 °C, and referenced relative to the residual proton resonances of C6D6 (δ= 7.15 ppm). The 11,13-*dicis* 6mr isomer was purified by normal-phase HPLC and 2.2 mg of the purified isomer was analyzed.

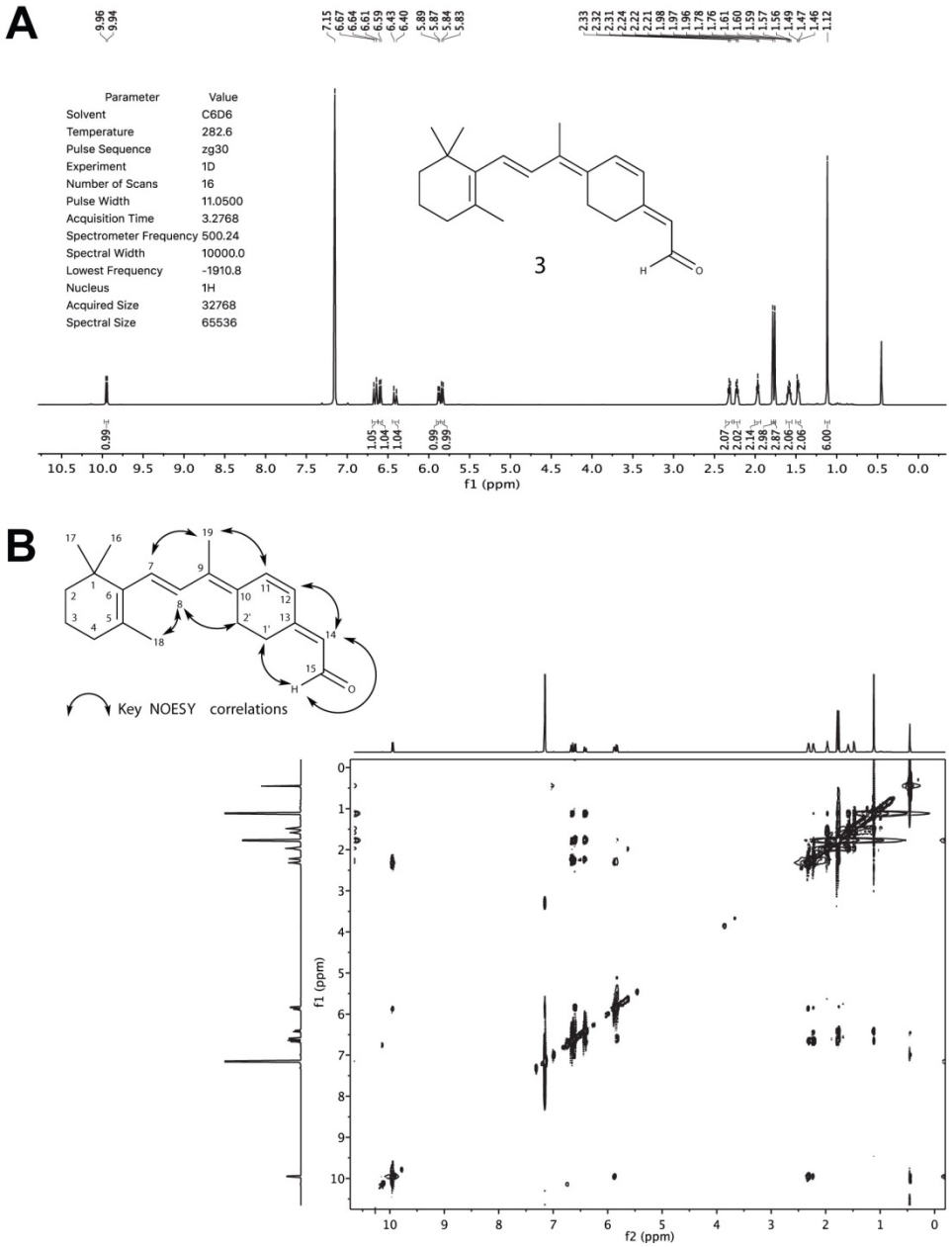

Figure S6. NMR characterization of the 11-*cis* isomer of 6mr (peak 3). ^{1}H (A) and NOESY (B) NMR spectra were acquired at 10 °C, and referenced relative to the residual proton resonances of C6D6 (δ= 7.15 ppm). The 11-*cis* 6mr isomer was purified by normal-phase HPLC and 2.4 mg of the purified isomer was analyzed.

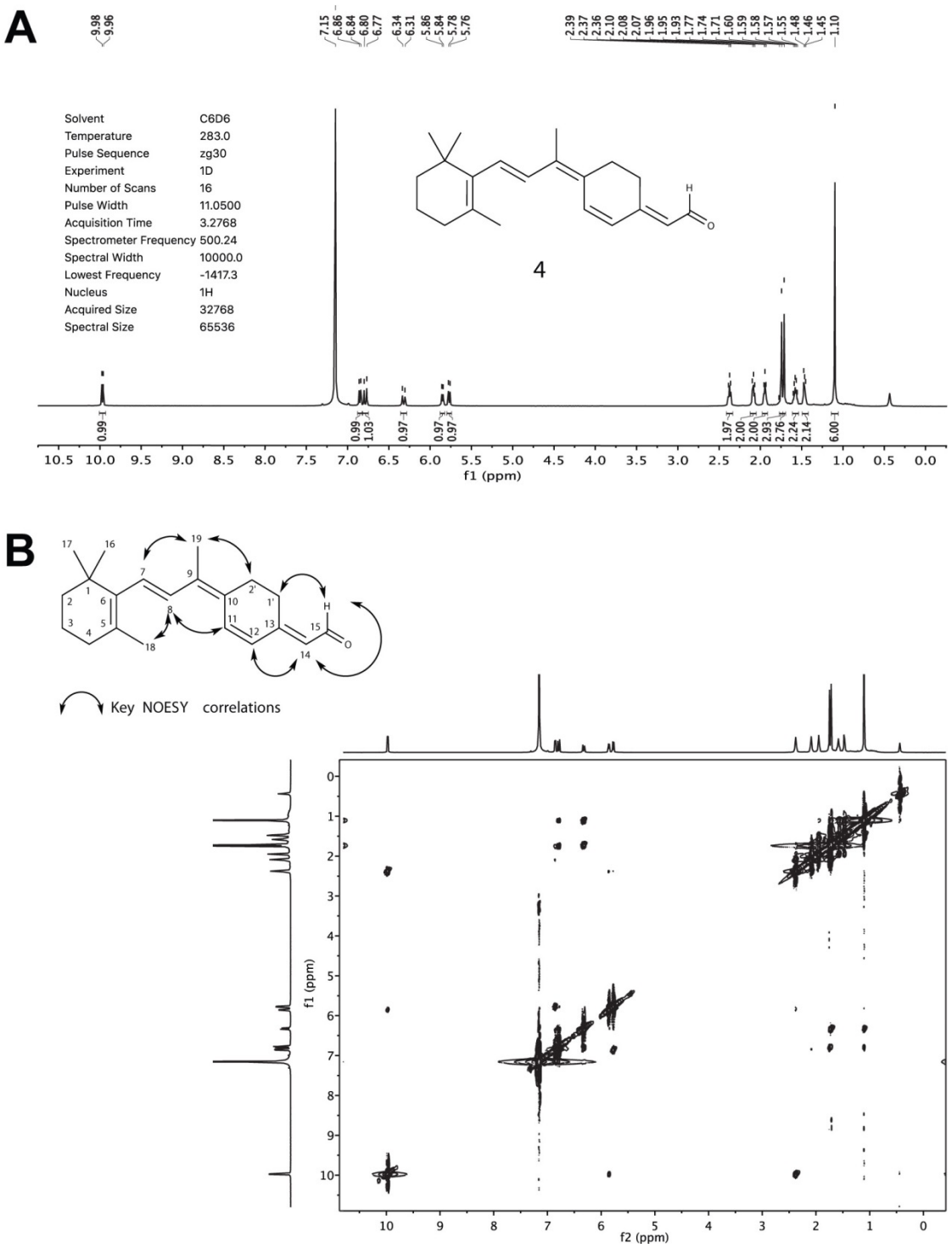

Figure S7. NMR characterization of the 9,11-*dicis* isomer of 6mr (peak 4). ^{1}H (A) and NOESY (B) NMR spectra were acquired at 10 °C, and referenced relative to the residual proton resonances of C6D6 (δ= 7.15 ppm). The 9,11-*dicis* 6mr isomer was purified by normal-phase HPLC and 2.1 mg of the purified isomer was analyzed.

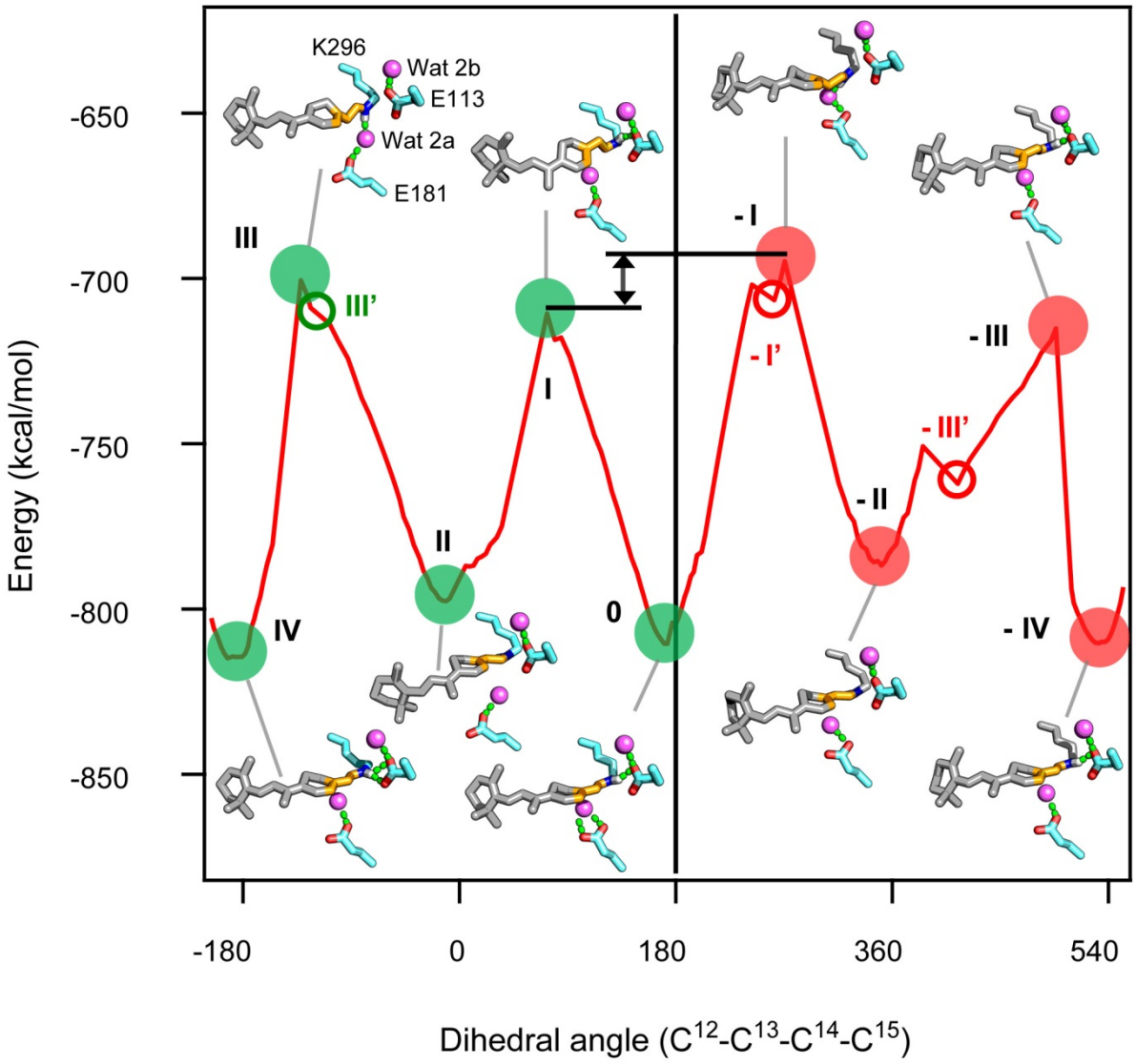

Figure S8. *In silico* thermal re-isomerization of Rh6mr. Energy plot of Rh docked with the 11-*cis* 6mr isomer during clockwise (*red circles*) and the preferred anticlockwise (*green circles*) rotation of the C^{12}-C^{13}-C^{14}-C^{15} dihedral angle of the 11-*cis* 6mr isomer. Wat 2a and 2b are shown as purple spheres and hydrogen bonds are depicted as dashed green sticks.

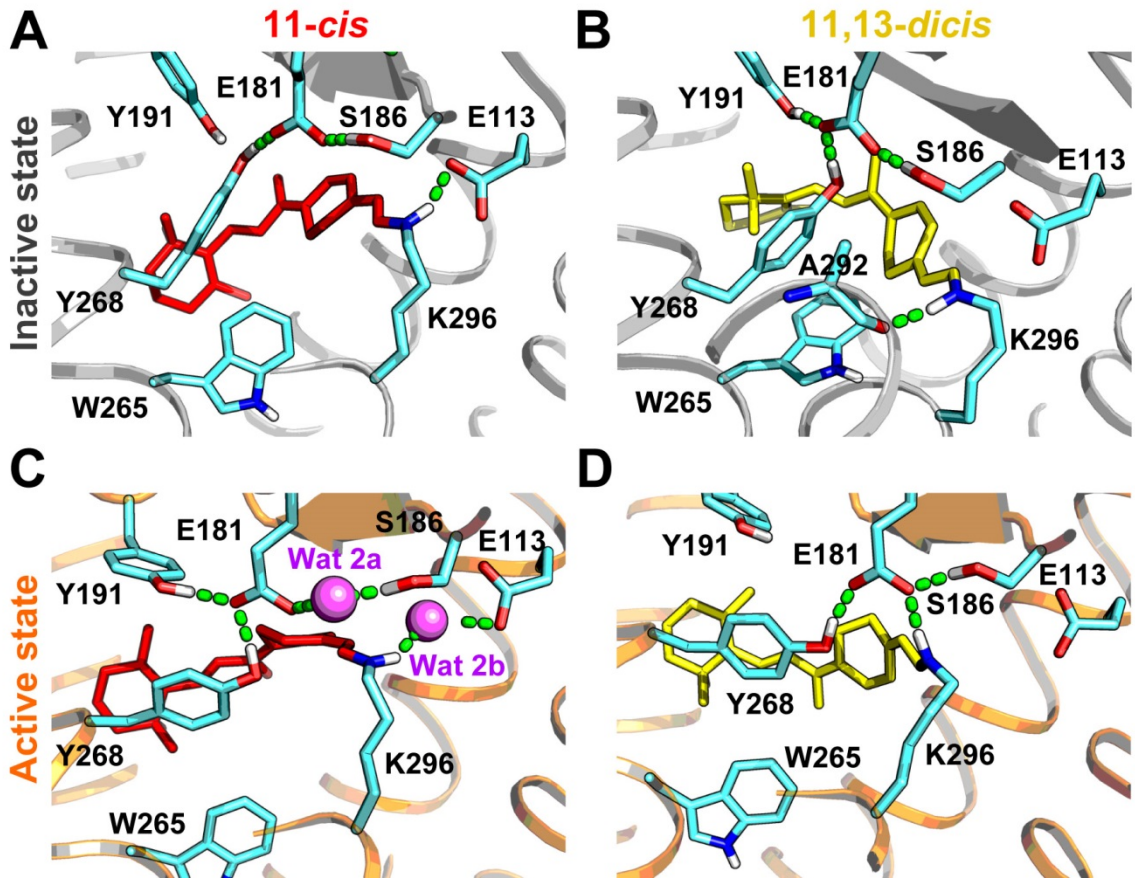

Figure S9. Molecular dynamic simulations of inactive Rh and the active Meta-II state docked with the 11-*cis* and the 11,13-*dicis* 6mr isomers. (A) Inactive Rh modeled with the 11-*cis* 6mr isomer. (B) Inactive Rh modeled with the 11,13-*dicis* isomer. (C) Active Meta-II state of Rh with the 11-*cis* isomer. The protonated Schiff base interacts with E113 via Wat 2b (*purple*). (D) Active Meta-II state with the 11,13-*dicis* isomer. Inactive Rh and active Meta-II are shown as grey and orange cartoons. The 11-*cis* and the 11,13-*dicis* isomers of 6mr are shown as red and yellow sticks, respectively. Wat 2a and 2b are shown as purple spheres and hydrogen bonds are depicted as dashed green sticks.

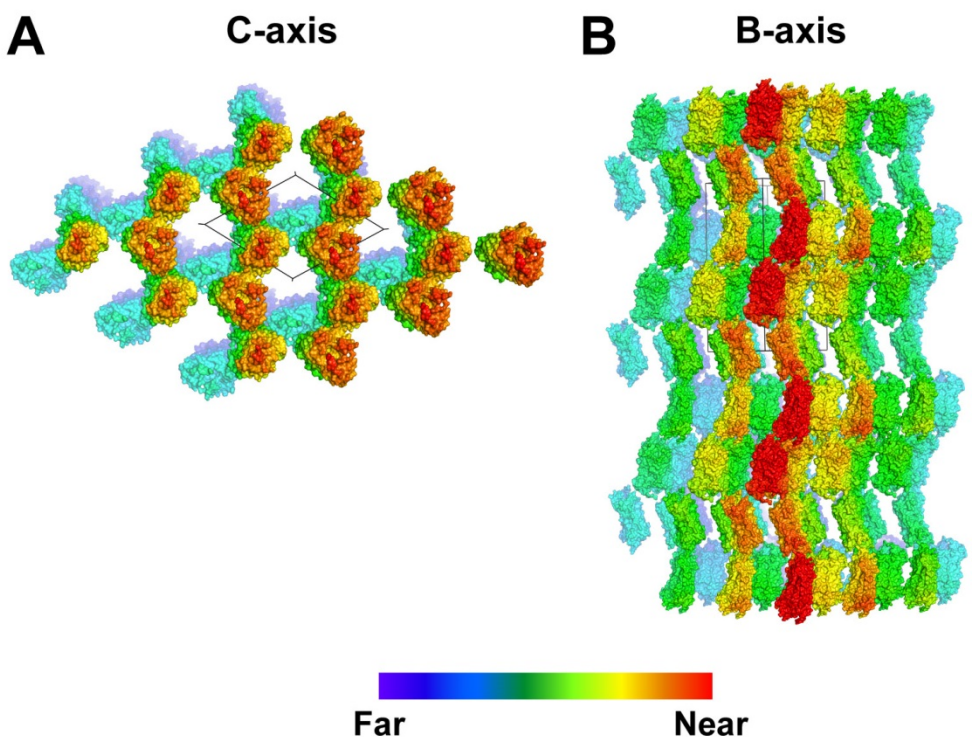

Figure S10. Crystal lattice packing of Rh6mr. Rh6mr was crystallized in a unique space group, $P3_121$, with protein molecules forming moderate crystal contacts with each other within the aqueous layers. (A) Top view along the long C-axis. Each asymmetric unit is composed of one Rh6mr molecule that forms crystal contacts with five neighboring molecules. (B) Side view along the smaller B axis.

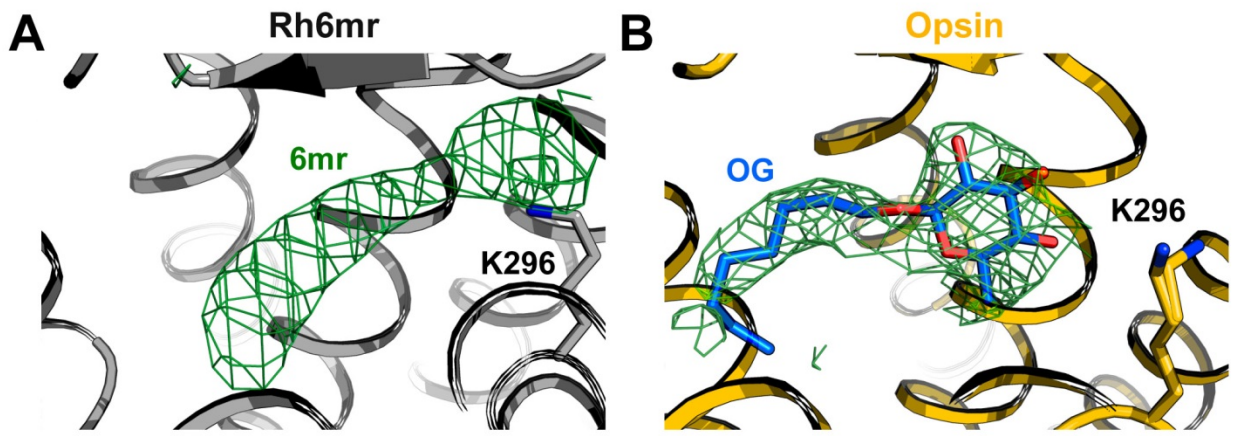

Figure S11. Comparison of Rh6mr and opsin binding pocket F_o-F_c omit maps**.** (A) F_o-F_c density of 6mr (1.9σ), observed in the Rh6mr crystal structure after the first round of REFMAC refinement. (B) Opsin binding pocket showing an F_o-F_c density corresponding to an *n*-octyl-β-D-glucopyranoside (OG) molecule (*blue*). The density was contoured at 1.9σ for comparison.

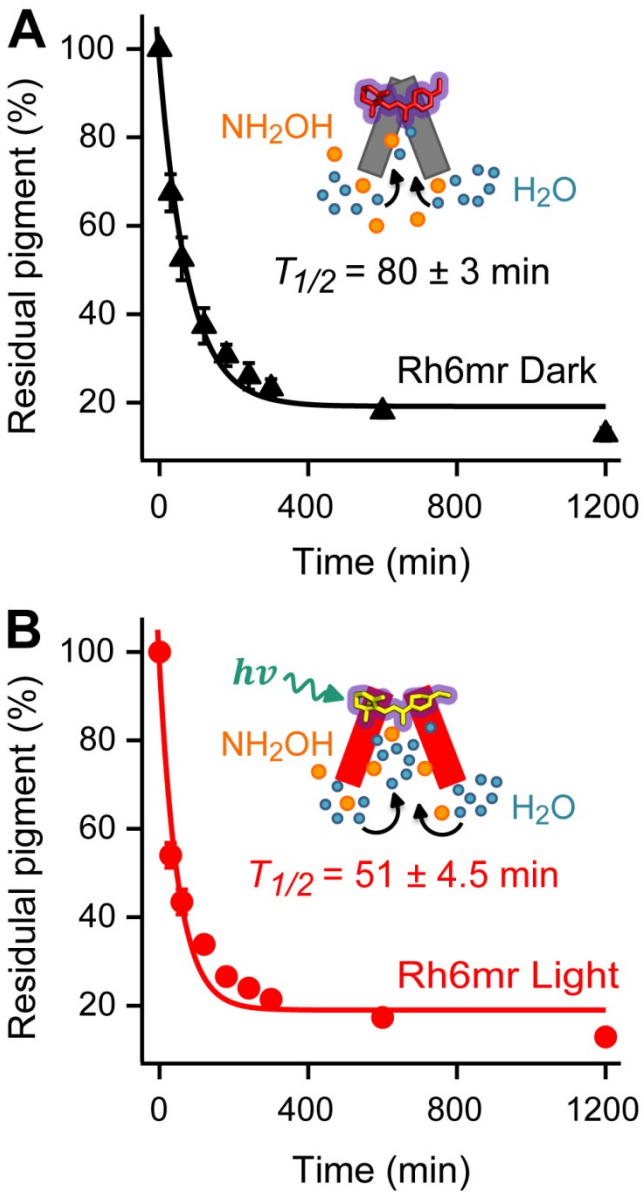

Figure S12. Susceptibility of Rh6mr to hydroxylamine in detergent micelles. Treatment of Rh6mr with 200 mM hydroxylamine resulted in a time-dependent release of 6mr from the retinal binding pocket as noted by the decrease in λ_{max} at 505 nm determined by UV-Vis spectroscopy. The data points for both dark and light conditions were plotted and subjected to single exponential fitting. The Rh6mr Schiff base hydrolysis rate was relatively slower in (A) the dark (*black line*) with a $T_{1/2}$ of 80 ± 3 minutes as compared to (B) the light conditions (*red line*) with a $T_{1/2}$ of 51 ± 4.5 minutes.

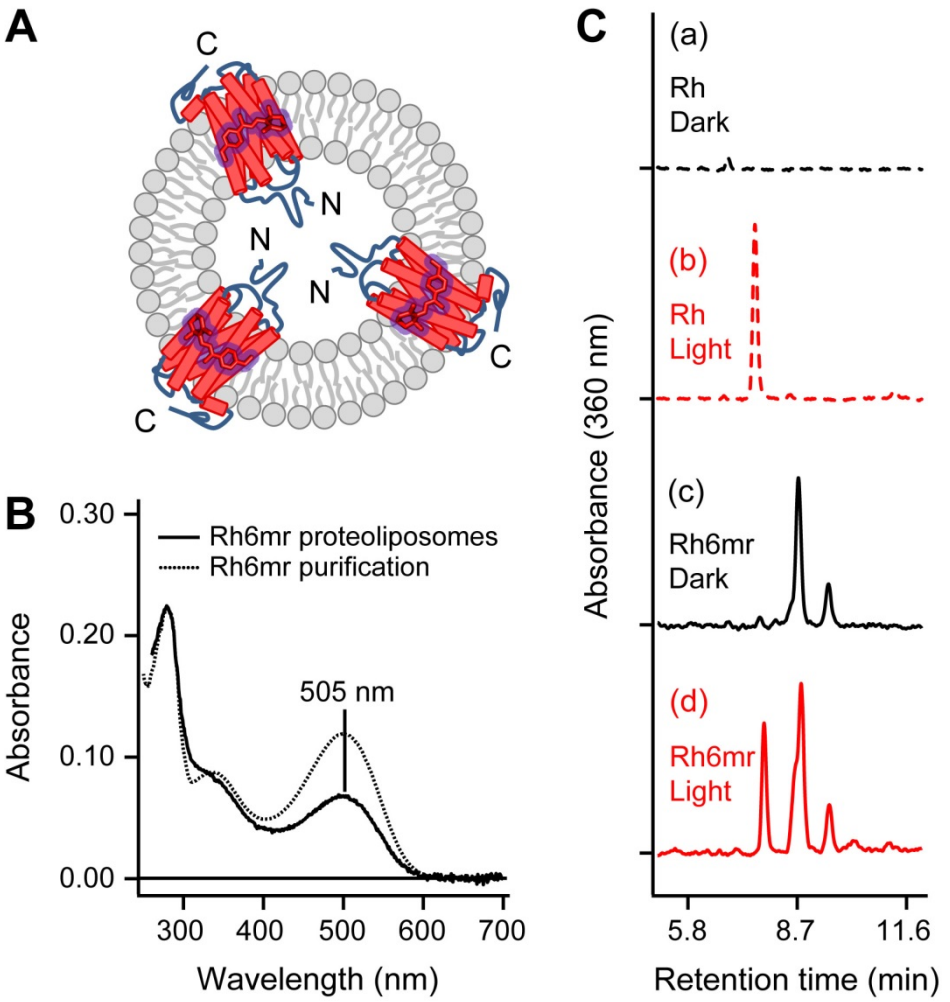

Figure S13. Bulk solvent entry into the cytoplasmic side of Rh6mr. (A) Schematic representation of the orientation of Rh6mr in proteoliposomes. (B) Characterization of Rh6mr proteoliposomes. The functional integrity of Rh6mr proteoliposomes was examined by their characteristic absorption peak at 505 nm in the dark. (C) Solvent entry determination by HPLC analysis of Rh and Rh6mr under non-denaturing conditions. Retinoid analysis of Rh liposomes treated with 200 mM hydroxylamine for 2 h in the dark (a) and after bleaching (b). Unlike Rh, treatment of Rh6mr proteoliposomes with 200 mM hydroxylamine in the dark for 2 h resulted in quantitative release of 6mr isomers (c). This suggests a relatively open cytoplasmic side of Rh6mr as compared to Rh, allowing solvent and hydroxylamine to gain access to the protonated Schiff base in the dark. Similar to Rh (b), hydroxylamine treatment of Rh6mr proteoliposomes in light conditions resulted in an increased liberation of the 6mr isomers (d). Quantitative comparison of Rh6mr proteoliposomal chromophore release under dark and illuminated conditions indicates further opening of the Rh6mr cytoplasmic side after illumination.

References

1. Bhattacharya S, Ridge KD, Knox BE, & Khorana HG (1992) Light-stable rhodopsin. I. A rhodopsin analog reconstituted with a non-isomerizable 11-cis retinal derivative. *J Biol Chem* 267(10):6763-6769.